Journal of Power Sources 306 (2016) 233–240

Contents lists available at ScienceDirect

Journal of Power Sources

journal homepage: www.elsevier.com/locate/jpowsour

Variation of coulombic efficiency versus upper cutoff potential of Li-ion cells tested with aggressive protocols

Jian Xia, Mengyun Nie, Lin Ma, J.R. Dahn*

Dept. of Physics and Atmospheric Science, 6300 Coburg Road, Dalhousie University, Halifax, Nova Scotia, B3H4R2, Canada

HIGHLIGHTS

- Coulombic efficiency depends on the cycling protocol and upper cutoff potential.
- Longer exposure, per cycle, to high V lowers coulombic efficiency.
- Longer exposure, per cycle, to high V does not increase short-term capacity fade.
- Oxidation products migrating to the negative electrode do not consume active Li.
- High V exposure causes an increase in cathode/electrolyte interface impedance.

ARTICLE INFO

Article history:
Received 5 October 2015
Received in revised form
5 December 2015
Accepted 7 December 2015
Available online 17 December 2015

Keywords:
High precision coulometry
Coulombic efficiency
Electrolyte oxidation
Impedance increase
Cell degradation

ABSTRACT

Three different cycling protocols including “continuous-cycling”, “barn-charge” and “cycle-store” were applied with an ultra high precision charger to $Li[Ni_{0.42}Mn_{0.42}Co_{0.16}]O_2$/graphite and/or $Li[Ni_{1/3}Mn_{1/3}Co_{1/3}]O_2$/graphite pouch cells tested using different upper cutoff potentials. The barn-charge and cycle-store protocols were designed so that cells stay at high potential for a larger fraction of their testing time compared to continuous cycling. For cells tested to 4.2, 4.4 or 4.5 V, the greater the fraction of testing time spent at high potential, the lower the coulombic efficiency and the greater the charge endpoint capacity slippage rate, with the effects being more severe at higher potential. These results confirm that $Li[Ni_{0.42}Mn_{0.42}Co_{0.16}]O_2$/graphite and $Li[Ni_{1/3}Mn_{1/3}Co_{1/3}]O_2$/graphite Li-ion cells which are charged and then left at high potential (>4.4 V) for extended periods of time will have much shorter calendar and cycle life compared to those that are continuously cycled as has been recently reported in long-term test results.

1. Introduction

There is an increasing demand for higher energy density Li-ion batteries. Charging the cells to higher potential is one of the simplest ways to achieve higher energy density, but this is normally at the expense of lifetime [1]. One major contributor to the poor life time is electrolyte oxidation at the positive electrode at high positive potentials [2,3]. Transition metal dissolution has also been suggested to play an important role [4].

There have been a considerable number of studies on how Li ion cells degrade and lose capacity at higher potentials [5–11]. Liao et al. [5] studied the self-discharge mechanism of $Li[Ni_{1/3}Mn_{1/3}Co_{1/3}]O_2$ NMC111/Li half cells at 4.2 V and 4.5 V and found that NMC111 undergoes a significant structural change, due to the transition metal dissolution, after cycling and storage at 4.5 V. Takei et al. [6] studied commercial 18,650-size $LiCoO_2$/graphite cells with different depths of-discharge and different state-of-charge and found that the rate of capacity degradation increased rapidly as the potential increased over 3.92 V. Choi et al. [7] studied 900 mAh wound prismatic $LiCoO_2$/graphite cells at different states-of-charge and found that high charge cut-off potentials and a long float-charge period at 4.2 V or above will rapidly accelerate cell degradation. It is believed that the major symptoms of cell degradation at high potential, e.g., capacity fade and impedance increase, originate from unwanted parasitic reactions at the positive electrode side and cells with higher potential operation will deteriorate more rapidly than cells that operate at lower potential [10,11].

The observations above strongly suggest that the cycle and

* Corresponding author.
E-mail addresses: jian.xia@dal.ca (J. Xia), niemengyun@gmail.com (M. Nie), L.Ma@dal.ca (L. Ma), jeff.dahn@dal.ca (J.R. Dahn).

http://dx.doi.org/10.1016/j.jpowsour.2015.12.013
0378-7753/

calendar life time of cells operated at high potential will depend strongly on the cycling protocol used. For example, one would expect cells tested in protocols with large fractions of time spent at high potential to perform worse than cells that spend small fractions of time at high potentials. A charging protocol study by Zhang et al. showed that cycle life of cells strongly depended on the charging protocol even if the same charging rate was used [12]. Detailed studies of the impact of the charging protocol on cell degradation are needed.

Evaluating the impact of upper cutoff potential as well as the cycling protocol on the lifetime of a Li-ion cell should include the careful measurements of coulombic efficiency (CE) [13]. Factors including the formation, growth, damage and repair of the solid electrolyte interphase films on both electrodes, electrolyte oxidation, electrolyte reduction, transition metal dissolution and damage to the positive electrode which impact cell lifetime will also impact the CE [14–16]. Using a Li inventory model, Smith et al. [15] considered the mathematical relationships between coulombic efficiency (CE), charge end-point capacity slippage, fade, and the parasitic currents. Based on the same model, Sinha et al. [28] investigated the mechanisms responsible for the voltage drop during storage and the capacity loss after storage. These results illustrated that the high precision experiments can be used to help elucidate cell degradation mechanisms during cycling or storage tests. Accurate measurements of the CE of Li-ion cells are extremely valuable to quantify the rates of parasitic side-reactions occurring at the electrolyte/electrode interfaces.

In this paper, three cycling protocols including continuous-cycling, “barn-charge” and “cycle-store” were designed to investigate the impact of the fraction of time spent at high potential on the life time of $Li[Ni_{0.42}Mn_{0.42}Co_{0.16}]O_2$/graphite and/or $Li[Ni_{1/3}Mn_{1/3}Co_{1/3}]O_2$/graphite pouch cells. Fig. 1 shows a schematic of the three cycling protocols that were used in this work. The fraction of time that cells that stay at high voltage increases from continuous-cycling to barn-charge to cycle-store protocols. The barn-charge protocol uses two currents, with the smaller current applied during the uppermost 200 or 300 mV of testing, yielding a voltage-time plot that resembles the top of a barn, hence the name. The cycle-store protocol, where cells are left at open circuit voltage for 20 h at the top of charge, was selected compared to a cycle-hold protocol because it is very difficult to measure the CE of cells with high accuracy when the current is changing in a constant potential hold. The impact of the various cycling protocols on CE, charge endpoint capacity slippage, cell impedance and gas evolution during testing were measured for tests conducted to 4.2, 4.4 and 4.5 V. Careful analysis of the ultra high precision charger results were made to determine whether charging to high potential impacted the rate of consumption of lithium in the negative electrode SEI or not.

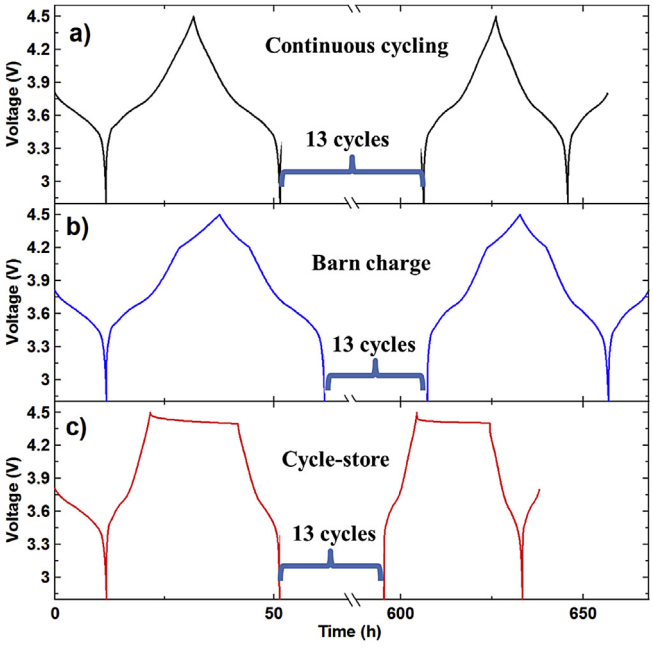

Fig. 1. Schematic of the three charge–discharge protocols that were used in this work.

2. Experimental

The pouch cells employed in this study were $Li[Ni_{1/3}Mn_{1/3}Co_{1/3}]O_2$ (NMC111)/graphite pouch cells with a capacity of 220 mAh balanced for 4.4 V operation and $Li[Ni_{0.42}Mn_{0.42}Co_{0.16}]O_2$ (NMC442)/graphite cells with a capacity of 180 mAh balanced for 4.7 V operation. The NMC442 (supplied by Umicore) had been surface coated with 3 wt. % of $LaPO_4$ (at 3M Co.) prior to electrode manufacturing. The pouch cells have a positive electrode area of 93.1 cm^2 and a negative electrode area of about 100.0 cm^2 which is larger due to electrode overhang. All pouch cells were manufactured by Li-Fun Technology (Zhuzhou, China), sealed without electrolyte in China then shipped to our laboratory in Canada. Cells were filled with electrolyte in Canada. The electrolyte was 1 M $LiPF_6$ in ethylene carbonate (EC)/ethyl methyl carbonate (EMC) (3:7 wt.% ratio, BASF, 99.99%) with 2 wt.% prop-1-ene-1,3-sultone as an electrolyte additive (PES, Lianchuang Medicinal Chemistry Co., Ltd., China, 98.20%). PES was chosen as the electrolyte additive because previous results showed that PES imparts similar performance to vinylene carbonate in NMC111/graphite pouch cells and because PES is beneficial in suppressing impedance growth and gas evolution in NMC442/graphite pouch cells tested to 4.2, 4.3 or 4.4 V [17–19].

Before filling with electrolyte, the cells were cut just below the heat seal and dried at 80 °C under vacuum for 14 h to remove any residual water. The cells were then transferred immediately to an argon-filled glove box for filling and vacuum sealing. The pouch cells were filled with 0.75 mL (0.90 g) of electrolyte. After filling, cells were vacuum-sealed with a compact vacuum sealer (MSK-115A, MTI Corp.). Then, cells were placed in a temperature box at 40.0 °C where they were held at 1.5 V for 24 h, to allow for the completion of wetting. Cells were then charged at 10 mA (~C/20) to 3.5 V. After that, cells were transferred into the glove box, cut open to release any gas generated and vacuum sealed again. The NMC442/graphite cells destined for 4.4 or 4.5 V operation were charged to 4.5 V at C/20 and degassed a second time at 4.5 V. These formation process and degassing potentials were selected based on *in-situ* gas evolution experiments, which showed that most of the gasses evolve in the formation step at potentials below 3.5 V and above 4.3 V [20].

The three different cycling protocols: “continuous-cycling”; “barn-charge” and “cycle-store” were carried out using the ultra high precision charger (UHPC) at Dalhousie University [21]. For continuous-cycling, cells were charged and discharged between 2.800 and upper cutoffs potentials of 4.200, 4.400 or 4.500 V) using currents corresponding to C/20 for 15 cycles. For barn-charge, cells were first charged to 4.200 V (or 4.000 V for 4.200 V operation) using currents corresponding to C/20. Then the charging current was switched to C/50 and applied up to the upper cutoff potential. After that, cells were discharged at C/50 to 4.200 V (or 4.000 V for 4.200 V operation) and then discharged to 2.800 V using currents corresponding to C/20. This procedure was then repeated 15 times on the UHPC. For the cycle/store protocol, cells were first charged to

upper cutoff potentials of 4.200, 4.400 or 4.500 V using currents corresponding to C/10, stored at open circuit 20.00 h and then discharged to 2.800 V using currents corresponding to C/10. This process was repeated for 15 cycles. The barn-charge and cycle-store protocols were designed so that the cells were exposed to higher potentials for significant fractions of their testing time. All pouch cells were cycled with clamps at 40 ± 0.1 °C. Comparisons between discharge capacity, coulombic efficiency and charge endpoint capacity slippage were made. Detailed information about the clamps used to apply pressure to the cells can be found in Ref. [22].

Gas generated during cycling was measured using Archimedes principle by weighing cells under nanopure water (18 MΩ) before and after UHPC cycling at room temperature [23]. All cells were charged or discharged to 3.80 V before weighing.

Electrochemical impedance spectroscopy (EIS) measurements were conducted on NMC442/graphite pouch cells after formation and after cycling on the UHPC [24]. Cells were charged or discharged to 3.8 V before they were moved to a 10.0 ± 0.1 °C temperature box. Alternating current (AC) impedance spectra were collected with ten points per decade from 100 kHz to 10 mHz with a signal amplitude of 10 mV at 10.0 ± 0.1 °C. A Biologic VMP-3 was used to collect these data.

Symmetric cells were made from electrodes obtained from some of these pouch cells after cycling. Symmetric cells were made by the procedures described by Petibon et al. and Burns et al. [24,25]. The pouch cells were charged or discharged to 3.80 V (approx. 50% state of charge) before they were opened in an argon-filled glove box. Six coin-cell size (1.54 cm^2) positive electrodes and six coin-cell size (1.54 cm^2) negative electrodes were cut from the pouch cells electrodes with a precision punch. Two negative symmetric coin cells, two positive symmetric coin cells and two full coin cells were reassembled using one polypropylene blown microfiber separator (BMF – available from 3M Co., 0.275 mm thickness, 3.2 mg/cm^2). The electrolyte used for symmetric cell was the same as that used in parent pouch cell. A positive electrode symmetric cell was constructed using two positive electrodes, and a negative electrode symmetric cell was constructed using two negative electrodes. A full coin cell was constructed using one positive electrode and one negative electrode.

3. Results and discussion

Fig. 2 shows the discharge capacity vs cycle number for the NMC111/graphite and NMC442/graphite pouch cells containing 2% PES undergoing the three cycling protocols. The capacity differences in the NMC442/graphite cells in Fig. 2b–d are due to the increasing upper cutoff potential from 4.2 V in Figure 2b to 4.5 V in Fig. 2d. Fig. 2 shows that cells cycled with charge-store protocol have lower capacity than the other two protocols at any cutoff potential due to the "self-discharge" that occurs during the 20 h storage period which is caused by electrolyte oxidation. When the upper cutoff potential was 4.5 V, the cells tested with charge-store protocol showed serious capacity fading near cycle 10, which was not seen for cells tested with "continuous-cycling" or "barn-charge" protocols. The dQ/dV vs. V curves (Fig. S1 in the supporting information) can also be used to examine the impact of the cycling protocols on cell degradation. Fig. S1 shows that the location and magnitude of the peaks change with the cut-off voltage and shift with the protocols used. Most clear is the impedance growth that occurs during charge-store protocol for the cells charged to 4.5 V.

Fig. 3 shows the coulombic efficiency (CE) vs cycle number for the same cells described in Fig. 2. Fig. 3 shows that the CE of the cells cycled at lower potential was closer to unity than the CE of cells cycled at higher potentials. This is because electrolyte oxidation accelerates at higher potential. Fig. 3 also shows that the CE of the cells was affected by the choice of cycling protocol. In all cases, cells that underwent the charge-store protocol had the lowest CE while the cells that underwent continuous cycling showed the highest CE. The lower CE of cells cycled with the charge-store protocol indicates that detrimental electrolyte oxidation continuously occurs during the extended period of time at high potential. Of course, the same reactions occur in the cells undergoing "continuous-cycling" or "barn-charge", but those cells are exposed to high potentials for a shorter period of time.

Fig. 4 shows the charge end-point capacity vs cycle number for the same cells described in Figs. 2 and 3. Many readers may not be familiar with graphs of charge endpoint capacity versus cycle number because only high precision chargers can measure this in a meaningful way. The paper by Burns et al. [26] defines what is meant by charge endpoint capacity slippage and shows the dramatic effect that electrolyte additives can have on it (See Figs. 1 and 3 in Ref. [25]). The charge endpoint capacity slippage rate was calculated from the slope of a best fit line to the final five points (cycles 11–15) of the charge endpoint capacity versus cycle number curve. For example, the charge endpoint capacities for one of the NMC111 cells undergoing continuous cycling were 235.977, 236.276, 236.522, 236.767 and 236.998 mAh from cycle 11 to cycle 15, respectively. The charge endpoint capacity slippage was calculated to be 0.253 mAh/cycle. Charge endpoint capacity slippage is caused by electrolyte oxidation reactions which can eventually deplete the cell of electrolyte leading to cell failure [27]. These are the same oxidation reactions that cause potential drop during storage. For example, Sinha et al. [28] have shown the excellent correlation between potential drop during storage and charge endpoint capacity slippage. Fig. 4 (notice the vertical axis spans are different in panels a, b, c and d). shows the dramatic increase of the charge endpoint capacity slippage rate with upper cutoff potential. The charge endpoint capacity slippage rate is also affected by the protocol used in the test. The clear trend is that the charge endpoint capacity slippage rate increases the longer fraction of time that the cells stay at higher potentials.

Fig. 5 shows the impedance spectra of the NMC111/graphite and NMC442/graphite pouch cells containing 2% PES after UHPC cycling for the three cycling protocols. The EIS tests were made at 10.0 °C and at 3.80 V. The diameter of the semicircle represents the sum of the charge-transfer resistances, R_{ct}, at both the positive and negative electrodes. What is called the charge transfer resistance (R_{ct}) in this paper for convenience includes the active particle-current collector contact resistance of both electrodes (small), the resistance to the transfer of Li^+ from the electrolyte to the electrode through the solid electrolyte interface (SEI) of both electrodes, and the electron transfer to the active material of both electrodes [29]. Fig. 5 shows that there are no obvious changes in the Nyquist spectra when the upper cutoff potential during cycling was below 4.4 V. Even after cycling at 4.5 V, the Nyquist spectra of cells using continuous-cycling or barn-charge protocols are very similar to those of the cells tested at 4.2 or 4.4 V (compare the inset in Fig. 5d to b and c). However, cells that underwent charge-store protocol during cycling to 4.5 V showed a massive impedance increase.

Figures S2a and S2b show a summary of the EIS results (R_{ct} measured from Fig. 5) and the volume change of the cells (swelling) data after UHPC cycling. Figure S2a shows again that the impedance of the cells increased greatly when cycle-store protocol was used with an upper cutoff of 4.5 V. The dramatic increase of impedance during cycle-store testing to 4.5 V is consistent with the results reported by Nelson et al. for cells tested in a similar manner to 4.5 V [30,31] Using symmetric cells, Nelson et al. showed this dramatic impedance increase originated from the positive electrode side. Figure S2b shows that significant gas production only occurs at

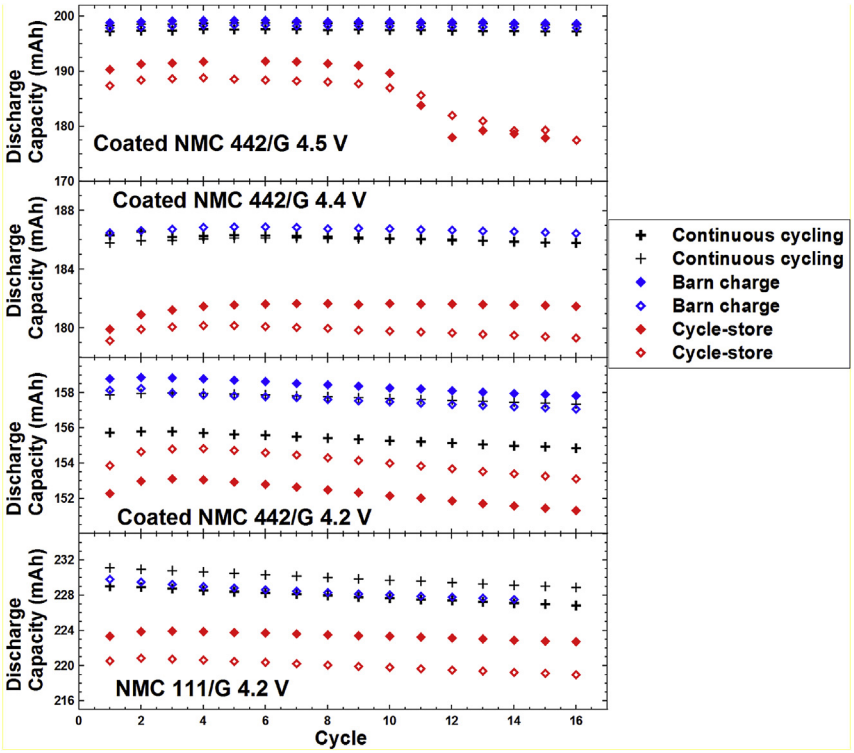

Fig. 2. Discharge capacity vs cycle number for the NMC111/graphite and NMC442/graphite pouch cells containing 2% PES undergoing the three cycling protocols shown in Fig. 1.

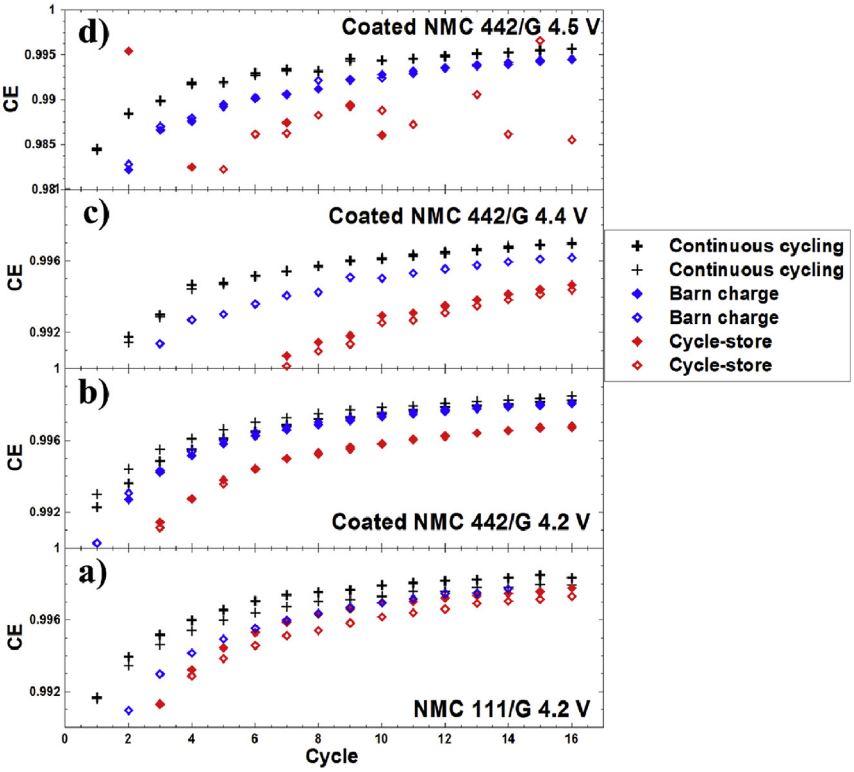

Fig. 3. Coulombic efficiency vs cycle number for the NMC111/graphite and NMC442/graphite pouch cells containing 2% PES undergoing the three cycling protocols shown in Fig. 1.

4.5 V when cycle-store or barn-charge protocols were used. Given that the initial volume of the pouch cells is 2.2 mL, the largest gas generation in Figure S2b is still less than 5% of the cell volume.

Table 1 gives a summary of the coulombic inefficiency (CIE = 1 − CE), charge endpoint capacity slippage and capacity fade measured during UHPC cycling for the NMC111/graphite and

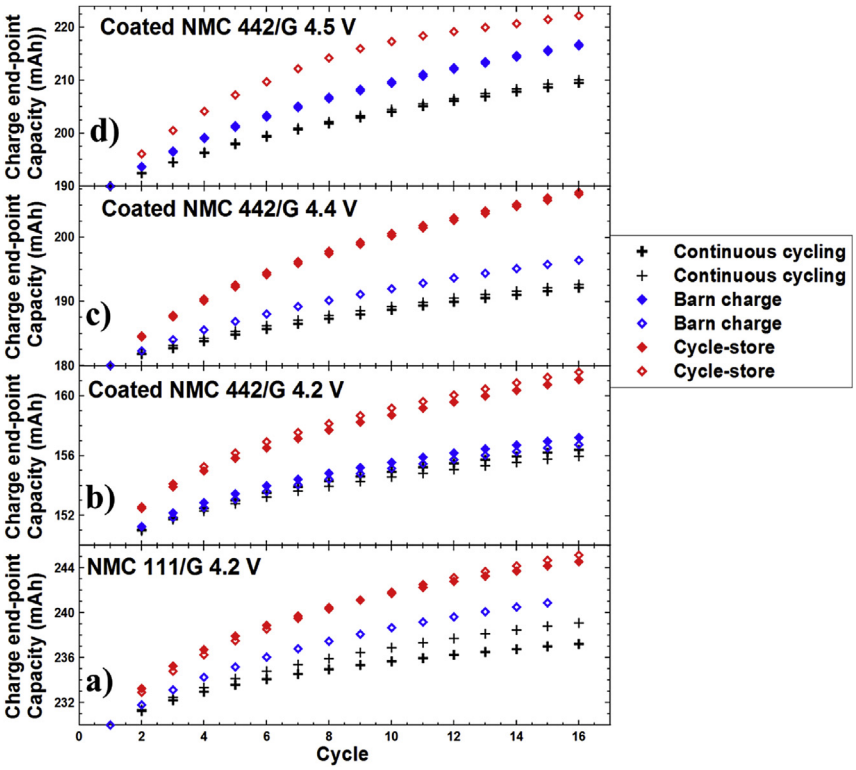

Fig. 4. Charge endpoint capacity vs cycle number for the NMC111/graphite and NMC442/graphite pouch cells containing 2% PES undergoing the three cycling protocols shown in Fig. 1.

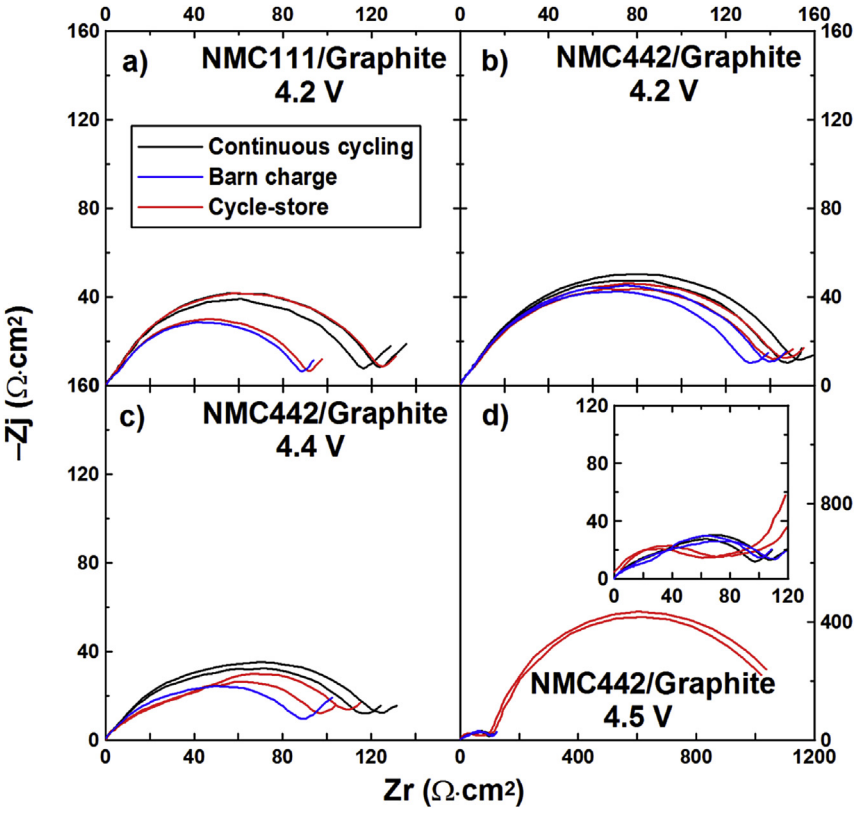

Fig. 5. Impedance spectra at measured at 3.8 V and at 10 ± 0.1 °C for (a) NMC111/graphite pouch cells tested to 4.2 V (b) NMC442/graphite pouch cells tested to 4.2 V, (c) NMC442/graphite pouch cells tested to 4.4 V, (d) NMC442/graphite pouch cells tested to 4.5 V. All cells contained 2% PES electrolyte additive and were tested according to the three cycling protocols shown in Fig. 1.

Table 1
$\Delta c/Q$, f/Q, $1\text{-}CE_{Cal}$ and $1\text{-}CE_{Mea}$ for the UHPC measurements on all different type of cells and different cycling protocols vs. voltage.

	NMC111/G 4.2 V				NMC442/G 4.2 V			
	$\Delta c/Q$	f/Q	$1\text{-}CE_{Cal}$	$1\text{-}CE_{Mea}$	$\Delta c/Q$	f/Q	$1\text{-}CE_{Cal}$	$1\text{-}CE_{Mea}$
Continuous- cycle	0.001344	0.000603	0.001947	0.001877	0.001518	0.0004	0.001918	0.001855
Barn-charge	0.001837	0.000533	0.002370	0.002264	0.001715	0.000458	0.002173	0.002106
Cycle-store	0.002288	0.000541	0.002829	0.002743	0.002612	0.000943	0.003555	0.003449
	NMC442/G 4.4 V				**NMC442/G 4.5 V**			
	$\Delta c/Q$	f/Q	$1\text{-}CE_{Cal}$	$1\text{-}CE_{Mea}$	$\Delta c/Q$	f/Q	$1\text{-}CE_{Cal}$	$1\text{-}CE_{Mea}$
Continuous- cycle	0.003056	0.000275	0.003331	0.003232	0.004632	0.00023	0.004862	0.004736
Barn-charge	0.003965	0.000256	0.004221	0.004073	0.005890	0.000246	0.006136	0.00596
Cycle-store	0.005951	0.000446	0.006255	0.006033				

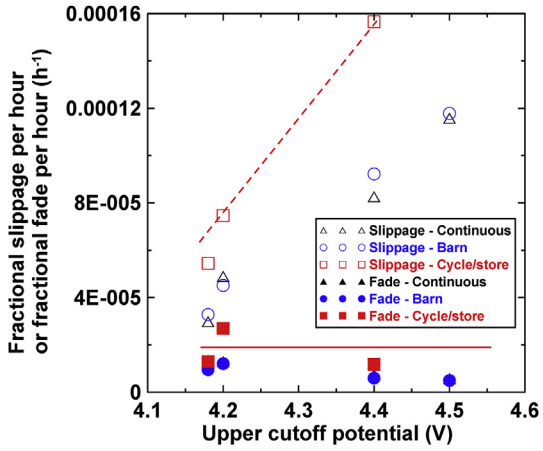

Fig. 6. Fractional charge endpoint capacity per hour (open symbols) and fractional fade per hour (filled symbols) for the NMC111/graphite and NMC442/graphite cells tested with the different protocols in Fig. 1 plotted versus the upper cutoff potential. The data for the NMC111/graphite cells which were charged to 4.2 V has been plotted at 4.18 V, for clarity, to avoid overlap with data for the NMC442 cells tested to 4.2 V.

NMC442/graphite pouch cells containing 2% PES undergoing the three cycling protocols. The CIE was calculated from the CE taken as an average of the final three data points (cycles 13–15) collected on the UHPC. The charge endpoint capacity slippage was calculated from the slope of a best fit line to the final five points (cycles 11–15) of the charge endpoint capacity versus cycle number [32].

Smith et al. [15] and Fathi et al. [33] consider how coulombic efficiency, charge endpoint capacity slippage and capacity fade should be related to each other. In the case where there is no positive electrode damage and no reduction of salt concentration in the electrolyte, the expected CE can be calculated by:

$$1 - CE = f/Q + \Delta_c/Q \quad (1)$$

where f is the capacity loss per cycle (mAh/cycle), Δ_c is the charge endpoint capacity slippage per cycle (mAh/cycle) and Q is the cell capacity (mAh). Table 1 shows Δ_c/Q, f/Q, $1 - CE_{Cal}$ and $1 - CE_{Mea}$ for the UHPC measurements on all cells with the various protocols tested to upper cutoff potentials of 4.2 V, 4.4 V and 4.5 V. The values of Δ_c/Q in Table 1 were obtained from the slopes of the last 5 data points in Fig. 4. The values of f/Q in Table 1 were taken from the slopes of the last 5 data points in Fig. 2. The values of $1 - CE_{Mea}$ in Table 1 were taken by averaging the last 3 data points in Fig. 3. The calculated values of $1 - CE_{Cal}$ in Table 1 were obtained using Equation (1). Table 1 shows that the calculated and measured values of 1-CE agree very well. Table 1 also shows that for 4.4 and 4.5 V testing, charge endpoint capacity slippage dominates the coulombic inefficiency as it is an order of magnitude larger than the fade.

In order to carefully compare the charge endpoint capacity slippage and fade for the three protocols, the values in Table 1 were divided by the time of a cycle so that the fractional slippage per hour and the fractional fade per hour could be directly compared from protocol to protocol. This division must be done because more fade and more slippage occur in a cycle that takes a longer time as discussed by Smith et al. [15]. Fig. 6 shows the fractional slippage per hour (open symbols) and the fractional fade per hour (filled symbols) plotted versus potential for the three protocols. Fig. 6 shows that the fractional slippage per hour increases dramatically with potential, while, by contrast, the fractional fade per cycle does not increase dramatically with potential (except the charge-store protocol at 4.5 V (see Fig. 2), which is due to the "rollover" failure of cells and that data is not included in Fig. 6 or Table 1). Fig. 6 also shows that the fractional slippage is much larger for the charge-

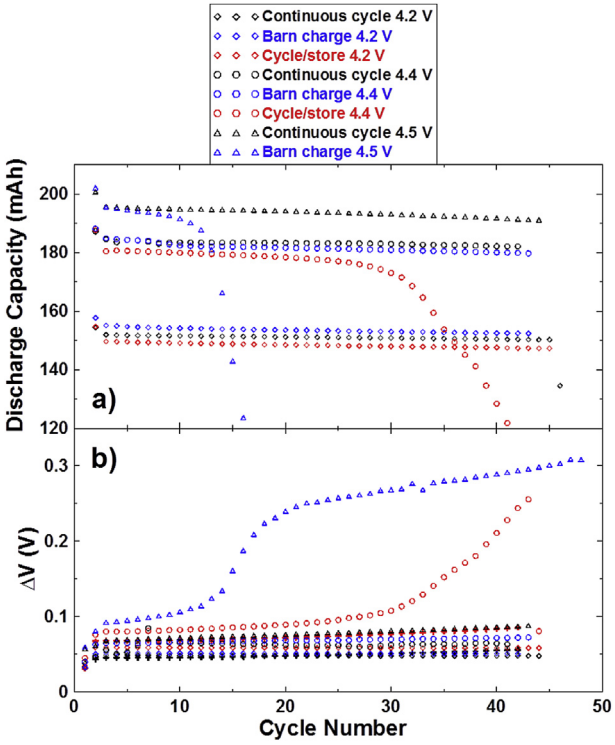

Fig. 7. (a) Discharge capacity and (b) ΔV, both plotted versus cycle number for the clamped clamped NMC442/graphite pouch cells containing 2% PES undergoing the three cycling protocols at 55 °C. The results in Fig. 7 are for the same cells from Fig. 2b,c and d. Testing to generate the results in Fig. 7 began after the completion of the UHPC cycles (Figs. 2–4), EIS measurements (Fig. 5) and gas volume measurements (Fig. S2) were made.

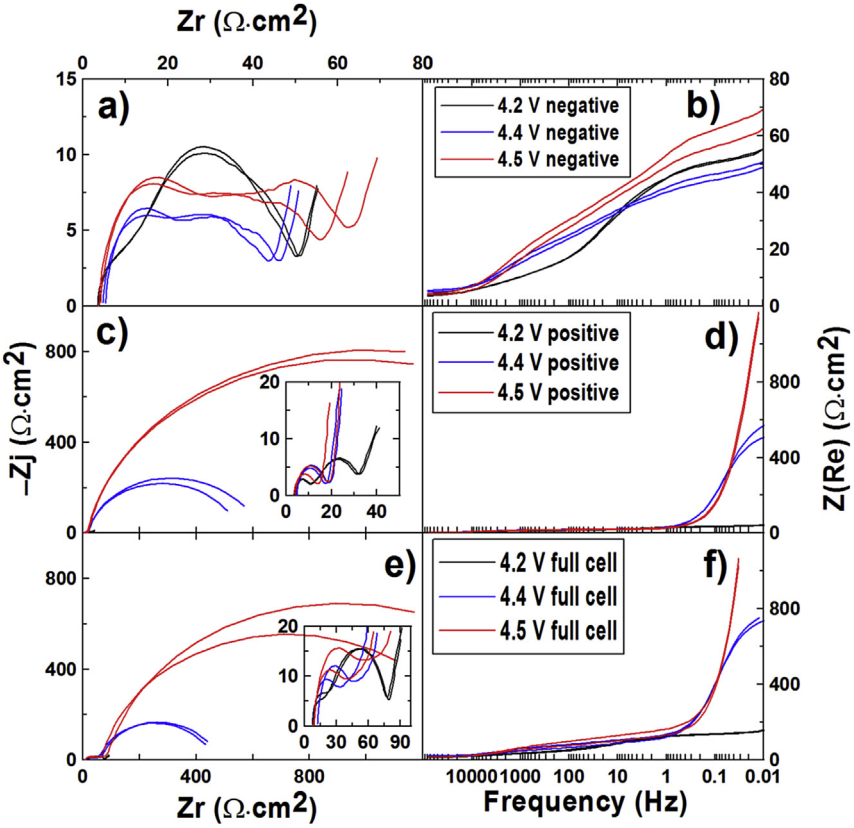

Fig. 8. The area-specific Nyquist plot and Bode plots of (a, b) negative electrode symmetric cells, (c, d), positive electrode symmetric cells and (e, f) full coin cells made from the NMC442 pouch cells after the long-term testing (Fig. 7) using the cycle/store protocol with different upper cutoff potentials.

store protocols than for the other protocols, presumably because the cells remain at high potential for extended times (20 h) during each cycle allowing a substantial amount of electrolyte oxidation to occur. Fig. 6 shows that the fractional fade per hour is worse for the cycle-store protocol than for the other protocols and that the fractional fade per hour during the UHPC testing actually decreases as the upper cutoff potential increases [Note: The error bars on the data points in Fig. 6 are less than the size of the data points.].

Why might the fractional fade per hour decrease as the potential increases? A speculative hypothesis is presented. At 4.2 V, transition metals, dissolved from the positive electrode may transport to the negative electrode and compromise the negative electrode SEI, as has been suggested for $LiMn_2O_4$/graphite cells operated at high temperature [34,35]. At higher potentials, electrolyte oxidation, possibly involving surface oxygen atoms from the NMC could cause the relatively rapid formation of a rock-salt surface layer that might be less prone to transition metal dissolution [36,37].

Fig. 6 shows that reactions during electrolyte oxidation at the positive electrode cause the charge endpoint slippage to increase with potential or with change of protocol, from continuous to barn to charge-store. Even with a dramatic increase in charge endpoint slippage, there is little impact on capacity fade which suggests that whatever species are created at the positive electrode these do not deplete the inventory of Li atoms that can transfer between the electrodes during cycling.

In order to demonstrate the strong negative impact of large charge endpoint capacity slippage (which "killed" the 4.5 V cycle-store cells after only 10 cycles during UHPC testing – see Fig. 2) the cells used for UHPC testing were put on long term testing at 55 °C using the same three protocols as implemented on a Neware (Shenzhen, China) battery tester. The Neware tester cannot measure charge endpoint capacity slippage or coulombic efficiency accurately, but it is well suited to measurements of capacity versus cycle number. Fig. 7a shows the capacity versus cycle number for eight representative NMC442/graphite cells tested under the three protocols to 4.2, 4.4 and 4.5 V Fig. 7 shows that all cells charged to 4.2 V functioned well for the 45 cycles tested. Cells tested with the cycle-store protocol to 4.4 V failed after about 30 cycles at 55 °C while cells tested with barn or continuous cycling to 4.4 V showed no capacity loss over the 45 cycles tested. For cells tested to 4.5 V, the cycle-store cells had already failed during UHPC testing, the cells undergoing barn cycling failed after 12 cycles while the continuously cycled cells had not failed after 45 cycles. At a particular upper cutoff potential, cell failure occurred (when it occurred, i.e. at 4.5 V) first for cycle-store protocol, then for barn protocol and finally for continuous cycling. This is in the order of which cells spent the largest fraction of testing time at the highest potential. Fig. 7b shows that the cell polarization, ΔV, (the difference between the average charge and average discharge potential) indicative of impedance growth, increased rapidly at the same time cells demonstrated rollover capacity failure.

Figures S3a and S3b show a summary of the EIS results and the gas evolution data after long-term cycling. The gas generation and the impedance growth during long-term cycling tests are extremely high at high voltages (see Fig. S3). Some of these cells were cut open in the glove box after the long-term cycling tests at 4.5 V and 55 °C. Figs. S4 and S5 show photographs of the electrodes and separators, respectively. Figs. S4 and S5 show that there is slight negative electrode delamination in the cells that underwent barn-charge and cycle-store protocol while the cells that underwent continuous cycling showed no delamination at all.

Fig. 8a,c and e show the area-specific Nyquist plots of negative

and positive electrode symmetric cells as well as full coin cells constructed from electrodes of the cycle-store pouch cells after the testing shown in Fig. 7. Fig. 8b,d and f show the Bode plots of the real area-specific impedance as a function of the logarithm of the frequency for the same cells. Fig. 8 shows that the impedance on the graphite electrodes does not change significantly as the upper cutoff potential increased while the impedance of the NMC442 electrode increased dramatically when the upper cutoff potential increased from 4.2 V to 4.5 V (about 30 times higher), presumably leading to the significant increase in the full cell impedance. Therefore, the cell degradation at high potential is mainly due to the deterioration of positive electrode/electrolyte interface while the contribution of negative electrode to the overall cell impedance is relatively small, which agrees well with the results presented by Abraham et al. [38].

4. Summary and conclusions

Ultra high precision coulometry studies of NMC111/graphite and NMC442/graphite pouch cells with three different cycling protocols have been made. These results should be of value to adopters of the high precision coulometry technique as they demonstrate that coulombic efficiency (CE) varies depending on the protocol used. Cells cycled to higher potentials have lower CE and higher charge endpoint capacity slippage rate than cells cycled at lower potentials. Cycling protocols like charge-store and barn, which increase the fraction of time that cells spend at higher potential, decrease the coulombic efficiency and increase the charge endpoint capacity slippage compared to continuous cycling, due to increased durations of electrolyte oxidation.

Even though charge endpoint capacity slippage or electrolyte oxidation per cycle increases with increasing upper cutoff potential or by changes to the cycling protocol, the short term capacity fade rate is virtually unaffected. This suggests that any products of electrolyte oxidation do not consume lithium from the inventory which can be cycled between the electrodes. Extended cycling to 4.4 or 4.5 V using the same three protocols showed that cells tested using cycle-store protocol failed first, those tested using barn protocol failed next and those using continuous cycling had not failed during the limited testing time. Cell failure was caused by impedance growth which symmetric cells showed occurred at the positive electrode.

These studies suggest that applications for NMC-based Li-ion cells involving long periods at potentials above 4.4 V may be challenging. Cycle protocols should be designed to minimize exposure of cells to high potentials. By contrast, researchers looking to develop high energy density NMC/graphite cells that can be charged to high potential should consider using protocols like cycle-store and barn, with UHPC or conventional testing equipment, to accelerate failure. That way, solutions like improved electrolytes or surface-coated positive electrode materials can be more rapidly screened.

Acknowledgment

The authors acknowledge the financial support of NSERC and 3M Canada under the auspices of the Industrial Research Chairs program. The authors thank Dr. Jing Li of BASF for providing some of the solvents and salts used in this work.

Appendix A. Supplementary data

Supplementary data related to this article can be found at http://dx.doi.org/10.1016/j.jpowsour.2015.12.013.

References

[1] Y.-K. Sun, Z. Chen, H.-J. Noh, D.-J. Lee, H.-G. Jung, Y. Ren, S. Wang, C.S. Yoon, S.-T. Myung, K. Amine, Nat. Mater. 11 (2012) 942.
[2] Z. Chen, Y. Qin, K. Amine, Y.-K. Sun, J. Mater. Chem. 20 (2010) 7606.
[3] L. Yang, B. Ravdel, B.L. Lucht, Electrochem. Solid-State Lett. 13 (2010) A95.
[4] G.G. Amatucci, C.N. Schmutz, A. Blyr, C. Sigala, A.S. Gozdz, D. Larcher, J.M. Tarascon, J. Power Sources 69 (1997) 11.
[5] X. Liao, Q. Huang, S. Mai, X. Wang, M. Xu, L. Xing, Y. Liao, W. Li, J. Power Sources 286 (2015) 551.
[6] K. Takei, K. Kumai, Y. Kobayashi, H. Miyashiro, N. Terada, T. Iwahori, T. Tanaka, J. Power Sources 97–98 (2001) 697.
[7] S.S. Choi, H.S. Lim, J. Power Sources 111 (2002) 130.
[8] J. Vetter, P. Novák, M.R. Wagner, C. Veit, K.-C. Möller, J.O. Besenhard, M. Winter, M. Wohlfahrt-Mehrens, C. Vogler, A. Hammouche, J. Power Sources 147 (2005) 269.
[9] M. Broussely, P. Biensan, F. Bonhomme, P. Blanchard, S. Herreyre, K. Nechev, R.J. Staniewicz, J. Power Sources 146 (2005) 90.
[10] K. Amine, C.H. Chen, J. Liu, M. Hammond, A. Jansen, D. Dees, I. Bloom, D. Vissers, G. Henriksen, J. Power Sources 97–98 (2001) 684.
[11] X. Wang, Y. Sakiyama, Y. Takahashi, C. Yamada, H. Naito, G. Segami, T. Hironaka, E. Hayashi, K. Kibe, J. Power Sources 167 (2007) 162.
[12] S.S. Zhang, J. Power Sources 161 (2006) 1385.
[13] T. Ohzuku, A. Ueda, N. Yamamoto, Y. Iwakoshi, 54, J. Power Sources (1995) 99.
[14] A.J. Smith, J.C. Burns, S. Trussler, J.R. Dahn, J. Electrochem. Soc. 157 (2010) A196.
[15] A.J. Smith, J.C. Burns, D. Xiong, J.R. Dahn, J. Electrochem. Soc. 158 (2011) A1136.
[16] A.J. Smith, J.C. Burns, X. Zhao, D. Xiong, J.R. Dahn, J. Electrochem. Soc. 158 (2011) A447.
[17] J. Xia, L. Ma, C.P. Aiken, K.J. Nelson, L.P. Chen, J.R. Dahn, J. Electrochem. Soc. 161 (2014) A1634.
[18] K.J. Nelson, J. Xia, J.R. Dahn, J. Electrochem. Soc. 161 (2014) A1884.
[19] L. Ma, J. Xia, J.R. Dahn, J. Electrochem. Soc. 161 (2014) A2250.
[20] C.P. Aiken, J. Self, R. Petibon, X. Xia, J.M. Paulsen, J.R. Dahn, J. Electrochem. Soc. 162 (2015) A760.
[21] T.M. Bond, J.C. Burns, D.A. Stevens, H.M. Dahn, J.R. Dahn, J. Electrochem. Soc. 160 (2013) A521.
[22] J. Xia, J. Self, L. Ma, J.R. Dahn, J. Electrochem. Soc. 162 (2015) A1424.
[23] C.P. Aiken, J. Xia, D.Y. Wang, D.A. Stevens, S. Trussler, J.R. Dahn, J. Electrochem. Soc. 161 (2014) A1548.
[24] R. Petibon, C.P. Aiken, N.N. Sinha, J.C. Burns, H. Ye, C.M. VanElzen, G. Jain, S. Trussler, J.R. Dahn, J. Electrochem. Soc. 160 (2013) A117.
[25] J.C. Burns, L.J. Krause, D.-B. Le, L.D. Jensen, A.J. Smith, D. Xiong, J.R. Dahn, J. Electrochem. Soc. 158 (2011) A1417.
[26] J.C. Burns, G. Jain, A.J. Smith, K.W. Eberman, E. Scott, J.P. Gardner, J.R. Dahn, J. Electrochem. Soc. 158 (2011) A255.
[27] J.C. Burns, N.N. Sinha, G. Jain, H. Ye, C.M. VanElzen, W.M. Lamanna, A. Xiao, E. Scott, J. Choi, J.R. Dahn, J. Electrochem. Soc. 159 (2012) A1095.
[28] N.N. Sinha, A.J. Smith, J.C. Burns, G. Jain, K.W. Eberman, E. Scott, J.P. Gardner, J.R. Dahn, J. Electrochem. Soc. 158 (2011) A1194.
[29] K.J. Nelson, G.L. Eon, A.T.B. Wright, L. Ma, J. Xia, J.R. Dahn, J. Electrochem. Soc. 162 (2015) A1046.
[30] K. Nelson, J.R. Dahn, ECS Conference on Electrochemical Energy Conversion & Storage with SOFC–XIV, abstract 457, Glasgow, July, 2015.
[31] K.J. Nelson, D.W. Abarbanel, J. Xia, Z. Lu, J.R. Dahn, J. Electrochem. Soc. 163 (2016) A272.
[32] J.C. Burns, A. Kassam, N.N. Sinha, L.E. Downie, L. Solnickova, B.M. Way, J.R. Dahn, J. Electrochem. Soc. 160 (2013) A1451.
[33] R. Fathi, J.C. Burns, D.A. Stevens, H. Ye, C. Hu, G. Jain, E. Scott, C. Schmidt, J.R. Dahn, J. Electrochem. Soc. 161 (2014) A1572.
[34] Y. Liu, X. Li, H. Guo, Z. Wang, Q. Hu, W. Peng, Y. Yang, Rare Met. 28 (2009) 322.
[35] M. Sano, T. Hattori, T. Hibino, M. Fujita, Electrochem. Solid-State Lett. 10 (2007) A270.
[36] Y. Kojima, S. Muto, K. Tatsumi, H. Kondo, H. Oka, K. Horibuchi, Y. Ukyo, J. Power Sources 196 (2011) 7721.
[37] S. Watanabe, M. Kinoshita, T. Hosokawa, K. Morigaki, K. Nakura, J. Power Sources 258 (2014) 210.
[38] D.P. Abraham, J.L. Knuth, D.W. Dees, I. Bloom, J.P. Christophersen, J. Power Sources 170 (2007) 465.